

A two-step ionospheric modeling algorithm considering the impact of GLONASS pseudo-range inter-channel biases

Rui Zhang^{1,6} · Yi-bin Yao² · Yue-ming Hu^{1,4,5} · Wei-wei Song³

Received: 20 September 2016 / Accepted: 27 April 2017 / Published online: 16 May 2017
© Springer-Verlag Berlin Heidelberg 2017

Abstract The Global Navigation Satellite System presents a plausible and cost-effective way of computing the total electron content (TEC). But TEC estimated value could be seriously affected by the differential code biases (DCB) of frequency-dependent satellites and receivers. Unlike GPS and other satellite systems, GLONASS adopts a frequency-division multiplexing access mode to distinguish different satellites. This strategy leads to different wavelengths and inter-frequency biases (IFBs) for both pseudo-range and carrier phase observations, whose impacts are rarely considered in ionospheric modeling. We obtained observations from four groups of co-stations to analyze the characteristics of the GLONASS receiver P1P2 pseudo-range IFB with a double-difference method. The results showed that the GLONASS P1P2 pseudo-range IFB remained stable for a period of time and could catch up to several meters, which cannot be absorbed by the receiver DCB during ionospheric modeling. Given the characteristics of the GLONASS P1P2 pseudo-range IFB, we proposed a two-step ionosphere modeling

method with the priori IFB information. The experimental analysis showed that the new algorithm can effectively eliminate the adverse effects on ionospheric model and hardware delay parameters estimation in different space environments. During high solar activity period, compared to the traditional GPS + GLONASS modeling algorithm, the absolute average deviation of TEC decreased from 2.17 to 2.07 TECu (TEC unit); simultaneously, the average RMS of GPS satellite DCB decreased from 0.225 to 0.219 ns, and the average deviation of GLONASS satellite DCB decreased from 0.253 to 0.113 ns with a great improvement in over 55%.

Keywords GLONASS · Ionospheric modeling · Pseudo-range inter-frequency bias

1 Introduction

TEC is a key parameter in the investigation of the spatial and temporal structure and variability of the ionosphere. Due to the dispersive nature of the ionosphere (Bassiri and Hajj 1992), it is an effective method for extracting the ionospheric delay and building an ionospheric model using dual-frequency GPS observations. In 1988, Lanyi and Roth (1988) first used GPS data and a third-order polynomial to model the regional ionospheric delay. Since then, various studies and applications in this area have been carried out (Schaer 1999; Camargo et al. 2000; Hernández-Pajares et al. 2011). Compared to other traditional ionospheric models, such as the Klobuchar, IRI, and GAIM (Klobuchar 1987; Bilitza and Reinisch 2008; Schunk et al. 2004) GPS-based ionospheric models exhibit a higher precision and resolution. Several international GNSS Service (IGS) analysis centers, including CODE (Center for Orbit Determination in Europe), JPL (Jet Propulsion Laboratory), UPC (Politechnical Uni-

✉ Yue-ming Hu
yueminghugis@163.com

¹ College of Natural Resources and Environment, South China Agricultural University, Guangzhou 510642, China

² School of Geodesy and Geomatics, Wuhan University, Wuhan 430079, China

³ Research Center of GNSS, Wuhan University, Wuhan 430079, China

⁴ Guangdong Province Key Laboratory for Land Use and Consolidation, Guangzhou 510642, China

⁵ Guangdong Province Engineering Research Center for Land Information Technology, Guangzhou 510642, China

⁶ Key Laboratory of the Ministry of Land and Resources for Construction Land Transformation, Guangzhou 510642, China

versity of Catalonia), and ESA (European Space Operations Centre), can provide a daily global ionosphere map (GIM) model, of which the product accuracy is within the range of $\pm 2\text{--}\pm 8$ TECu (Hernández-Pajares et al. 2009).

However, the TEC derived from GPS signals is badly affected by the DCB, of both the satellites and receivers (Mannucci et al. 1998); the DCB represents a difference between the measurements on two or more frequencies and may cause several meters of error if not managed appropriately. In general, the DCB is considered an instrumental error because it is caused by the analog hardware delays of the satellite and receiver (Arikan et al. 2008; Håkansson et al. 2016). In spite of the fact that the estimated DCB values may be dependent on the hardware temperature (Heise et al. 2005) or geometric conditions (Hong et al. 2008), the satellite and receiver DCB values are often assumed to be constant for 1 day (or even longer) to simplify calculations; these values are estimated along with the model coefficients using the least squares method (Jin et al. 2008). The above-mentioned IGS analysis centers also provide the DCB product of various satellites and several tracking stations.

With the full operation of GLONASS with 24 satellites since December 8, 2011, and the improved quality of GLONASS orbits and clocks (Dow et al. 2009), combined GPS/GLONASS applications have become increasingly popular. Unlike GPS, the present GLONASS navigation system uses FDMA to make the signals from individual satellites distinguishable (Wanninger et al. 2007), which leads to different wavelengths and IFBs for both pseudo-range and carrier-phase observations. Many studies have analyzed the features of carrier-phase IFBs, which are proved to be linear functions of the frequency (Kozlov et al. 2000; Zinoviev 2005; Yamanda et al. 2010; Al-Shaery et al. 2013). Only a few studies analyzed the characteristics of pseudo-range IFBs, and the results indicated that pseudo-range IFBs can reach up to several meters (Tsuji et al. 2000; Al-Shaery et al. 2013; Chuang et al. 2013). However, these researchers mainly focused on one frequency observation (P1 or P2) or the ionosphere-free combinations, seldom considering the differences of P1 and P2 pseudo-range IFB. There are a few researchers who discussed the method and effects of using GLONASS observations to establish an ionosphere model (Jakowski et al. 2002; Kunitsyn et al. 2011); their modeling algorithms were similar to those for the GPS and did not consider the P1P2 pseudo-range IFB influences. CODE is the only analysis center that uses both GPS and GLONASS observations to generate a daily GIM model (Hernández-Pajares et al. 2009).

For the purpose of effectively separating the ionospheric delay from the satellite and receiver hardware delay, it is necessary to analyze the GLONASS P1P2 pseudo-range IFBs property. In this paper, we obtained data from four groups of co-location GLONASS stations with different receiver and

antenna types; our analysis of the results showed that the GLONASS P1P2 pseudo-range IFB must be removed during ionospheric modeling. We propose a new two-step ionospheric modeling algorithm using the prior IFB information. The experimental analysis showed that the new algorithm reduced the systemic bias of the ionospheric product and significantly increased the accuracy of the GLONASS satellite DCB product.

2 GNSS ionospheric modeling algorithm

Without taking into consideration the higher-order ionospheric effect, the anisotropic ionospheric plasma effects in the phase and pseudo-range delays at high frequencies can be represented as a rapidly decreasing series of the inverse powers of frequency (Kim and Tinin 2011). The basic mathematical model of the GNSS carrier-phase and pseudo-range observations are shown in Eqs. (1) and (2) in units of length:

$$P_r^s = \rho + c(dt - dT) - \frac{A}{f_m^2} + T + D_r + D^s + \varepsilon_P, \quad (1)$$

$$L_r^s = \rho + c(dt - dT) + \frac{A}{f_m^2} + T + \lambda_m N + \varepsilon_L. \quad (2)$$

In Eqs. (1) and (2), P_r^s and L_r^s represent the pseudo-range and phase measurements of the receiver transmitter at a given time, respectively; ρ , dt , and dT are the corresponding distance, receiver, and satellite clock errors; A represents the slant of the total electron content (STEC); T represents the slant tropospheric delay; f_m refers to the frequency of the observations; D_r and D^s are the receiver and satellite DCBs, respectively; λ_m represents the wavelength of the carrier observations; N represents the carrier-phase ambiguity in cycles (including the integer number and float phase instrumental delays); and ε_P and ε_L are the observational noises.

We obtained the relevant ionospheric delay measurement by using Eqs. (1) and (2) with different frequency observations from the same satellites:

$$P_4 = P_1 - P_2 = \frac{A}{f_2^2} - \frac{A}{f_1^2} + ((D_1^r - D_2^r) + (D_1^s - D_2^s)), \quad (3)$$

$$L_4 = L_2 - L_1 = \frac{A}{f_2^2} - \frac{A}{f_1^2} - (N_1 - N_2). \quad (4)$$

According to Eqs. (3) and (4), TEC can be calculated directly using pseudo-range or phase observations. However, the pseudo-range observations are significantly influenced by measurement noise, and the phase observation method will introduce ambiguous parameters, which cause high computational complexity. Therefore, TEC is usually calculated using the phase smoothing pseudo-range algorithm (Lachapelle

et al. 1986). Due to the strong correlation, it is hard to separate D_1^r from D_2^r . $D_1^r - D_2^r$ is often seen as a constant parameter and estimated during ionospheric modeling (which is the same for $D_1^s - D_2^s$). In order to simplify the description of the ionospheric distribution, it is often assumed that the ionospheric delay is concentrated at an infinitely thin layer at a certain height above the earth, so that the total electron content can be seen as a physical quantity with location and time distribution characteristics; it is described as a function with the location and time as its independent variables. There are several fitting functions available: polynomials, triangular interpolation, or spherical harmonic model (Wild 1994; Mannucci et al. 1993; Schaer 1999). Eq. (5) is the general form of the GNSS ionospheric model using the spherical harmonic function:

$$STEC(\beta, s) = \sum_{n=0}^{n_{max}} \sum_{m=0}^n \tilde{P}_{nm}(\sin \beta)(a_{nm} \cos ms + b_{nm} \sin ms)/M + D^s + D^r, \tag{5}$$

where β and s represent the geomagnetic latitude and sun-fixed longitude of the user IPP, \tilde{P}_{nm} is the regular Legendre series, a_{nm} and b_{nm} are coefficients to be estimated, n_{max} is the maximum degree of the spherical harmonic expansion, and M represents the mapping function.

In (5) the station and the satellite DCB parameters are strongly correlated, and cannot be isolated directly. A common approach to solve the problem is adding constraints for each satellite system to force the sum of all satellite DCBs equal to zero, which will not affect the relative DCB values for each satellite system.

$$\sum_{n=0}^{n_{GPS}} D_G^s = 0, \quad \sum_{n=0}^{n_{GLONASS}} D_R^s = 0. \tag{6}$$

3 GLONASS pseudo-range IFB impact analysis

In the traditional GNSS ionospheric algorithm, $D_1^r - D_2^r$ is often seen as a constant value for each receiver. However, for the GLONASS receivers, the pseudo-range deviations between the frequencies may be absorbed by the receiver hardware delay variation, resulting in variations in the D_1^r , D_2^r for the different GLONASS satellites, and the $D_1^r - D_2^r$ may also be different. The process of ionospheric modeling may introduce errors and affect the ionosphere model if the parameters are processed as those as the traditional algorithms.

From Eq. (3), we can see that it is difficult to distinguish $D_1^r - D_2^r$ for a single station because of the ionospheric delay and $D_1^s - D_2^s$. However, most of these errors can be removed by using the co-location (or distance ultra short)

GPS/GLONASS data through a single difference between the stations, only remaining $\Delta(D_1^r - D_2^r)$.

$$\Delta(D_1^r - D_2^r) = P_4^{r1} - P_4^{r2}. \tag{7}$$

If the receiver P1P2 hardware delay is the same for all the satellites, then $\Delta(D_1^r - D_2^r)$ should be a fixed value for all satellites between two stations. Otherwise, the GLONASS P1P2 pseudo-range IFB must be considered in the process of the ionosphere modeling.

Seven stations were chosen to build four groups of GLONASS co-location stations; the station distribution, receiver, and antenna types are shown in Table 1.

Figure 1 shows the $\Delta(D_1^r - D_2^r)$ time series of PRN02 at stations mobk and mobj together with the elevation. Although the pseudo-range differential amplified the observation noise, the results generally showed a good agreement at elevation angles above 30° for duration of one day. The daily $\Delta(D_1^{\wedge} - D_2^r)$ value was estimated using the elevation weighting method:

$$\Delta(D_1^{\wedge} - D_2^r) = \frac{\sum P \cdot \Delta(D_1^r - D_2^r)}{\sum P}, \tag{8}$$

where P represents the observations' weights which were determined as follows, Ea represents the elevation,

$$ea = \sin^2(Ea) \begin{cases} \text{if}(Ea > 30^\circ) & P = 10 \times ea \\ \text{else} & P = ea \end{cases} \tag{9}$$

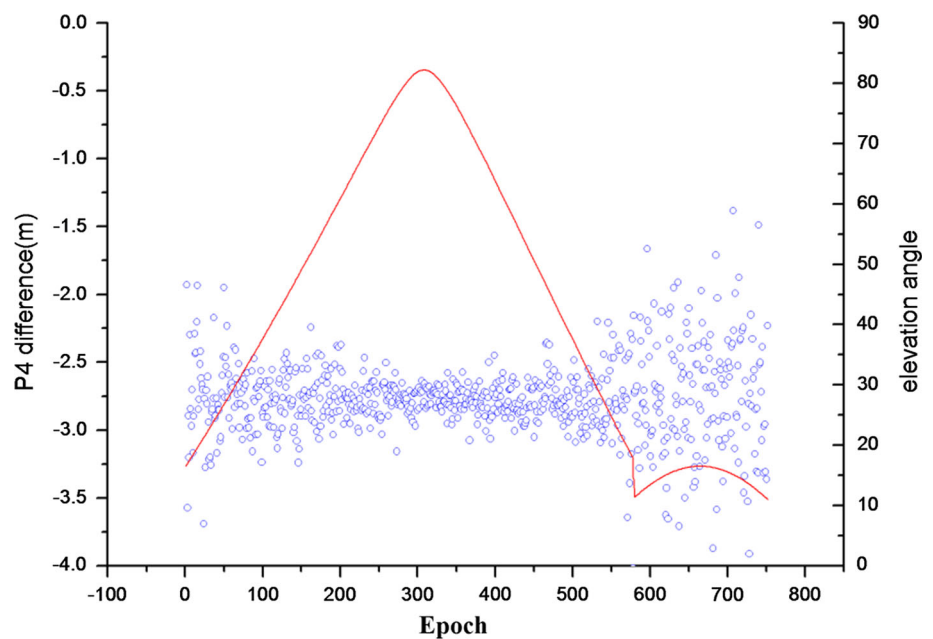
Figure 2 shows the daily $\Delta(D_1^{\wedge} - D_2^r)$ estimated values of PRN02 and PRN08 together with the number of observations. The monthly changes of the satellites were quite stable. The average $\Delta(D_1^{\wedge} - D_2^r)$ value for the PRN02 satellite was 2.278 m and the standard deviation (STD) was 0.024 m; for PRN08, the average value was 2.592 m, and the STD was 0.026 m. Figure 3 shows the daily $\Delta(D_1^{\wedge} - D_2^r)$ values and variations for all observed satellites.

According to Fig. 3, the monthly estimation accuracy for each satellite was better than 0.05 m (95% confidence level). However, the maximum deviation between the satellites was up to about 1 m, which far exceeded the estimation error. It may be assumed that the receiver pseudo-deviations between P1 and P2 frequencies were different for the mobk and mobj stations. Next, the data of the four groups of station combinations were analyzed. Prior research has proven that GLONASS phase IFBs are frequency dependent (Zinoviev 2005; Wanninger 2012). Figure 4 shows the $\Delta(D_1^{\wedge} - D_2^r)$ values and variations together with the GLONASS RF channels.

Figure 4 shows that the variation characteristics and frequency correlations for four groups of GLONASS co-

Table 1 Station distribution, receiver, and antenna types of selected GLONASS receivers

Group	Station	X(m)	Y(m)	Z(m)	Distance(m)	Receiver Types	Antenna Types
1	mobj	2936424.499	2178374.114	5208858.471	0.011	JPS LEGACY	JPSREGANT_SD_E
	mobk	2936424.503	2178374.119	5208858.480		JPS EGGDT	JPSREGANT_SD_E
2	tixi	-1264873.323	1569455.771	6031003.408	0.196	JPS EGGDT	TPSCR3_GGD
	tixg	-1264873.390	1569455.717	6031003.232		TPS ODYSSEY_E	TPSCR3_GGD
3	godn	1130760.87	-4831298.654	3994155.163	76.024	JAVAD TRE_G3TH	TPSCR.G3
	gods	1130752.307	-4831349.086	3994098.923		JAVAD TRE_G3TH	TPSCR.G3
4	godz	1130773.639	-4831253.559	3994200.438	141.017	JPS EGGDT	AOAD/M_T

Fig. 1 $\Delta(D_1^r - D_2^r)$ time series of PRN02, at stations mobk and mobj, DoY080, 2012

location station combinations, which exhibited significant differences between the satellites. For the gdsn station combination (godn and godz), with the same receiver and antenna, the $\Delta(D_1^r - D_2^r)$ values of all satellites were remarkably consistent, ranging within -0.6 to -0.3 m; the deviations of each satellite group with same frequency were generally less than 0.05 m. The $\Delta(D_1^r - D_2^r)$ values for the tix station combination (tixi and tixg) with different receivers showed significant frequency-dependent trends. However, for both the mob (mobj and mobk) and gdsz (gods and godz) combi-

nations, the $\Delta(D_1^r - D_2^r)$ values varied greatly between the satellites and showed no significant linear relationship with the frequencies

4 A new two-step ionospheric modeling algorithm

The analysis results above indicate that the GLONASS P1P2 pseudo-range IFB remained stable for a period of time and was different for each satellite, which cannot be absorbed

Fig. 2 Daily $\Delta(D_1^r - D_2^r)$ estimated values of PRN02 and PRN08 at stations mobk and mobj, from DoY 031 to DoY 060, 2012

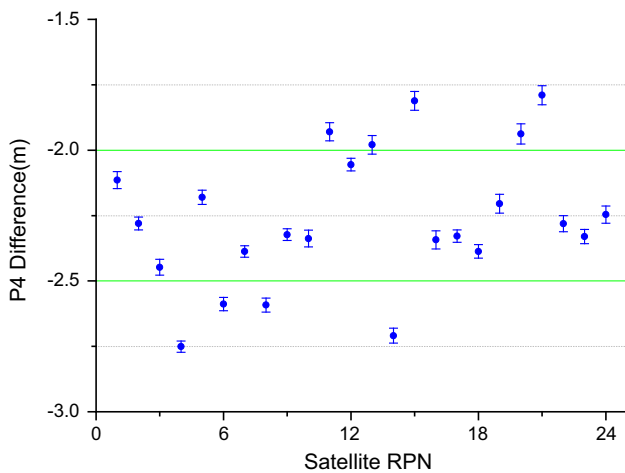
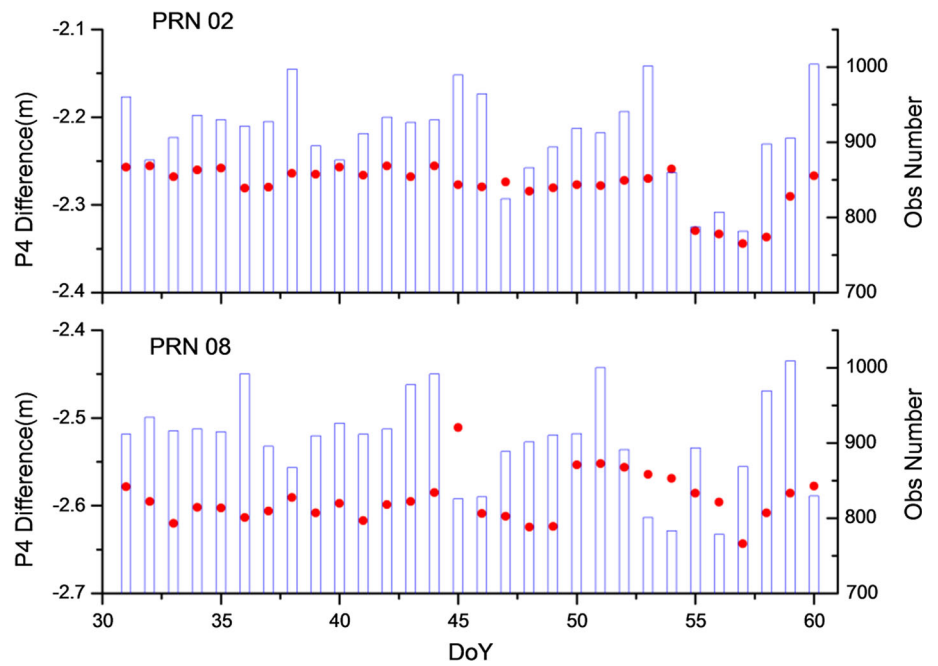


Fig. 3 Monthly $\Delta(D_1^r - D_2^r)$ values and variations of all GLONASS satellites at stations mobk and mobj

in the receiver DCB during ionospheric modeling. The IFB deviations showed a certain relevance to the satellite frequency for certain types of receivers and antennas, but this phenomenon was not universal and made it impossible to express the IFB with the frequency as an independent variable. It is also inappropriate to estimate the receiver DCB for each satellite as the traditional method, which would lead to excessive parameterization and affect the efficiency of the estimation efficiency.

In this paper, we proposed a new two-step ionospheric modeling algorithm with prior IFB information. Firstly, for a tracking station network, a station with a good location and observation environment was chosen as the reference station.

Secondly, using the above method, the $\Delta(D_1^r - D_2^r)$ values of all satellites between the reference and rover stations were estimated.

For the parameter estimation process, the traditional ionospheric model (such as Eq. (5)) can be simplified as:

$$STEC = AX = \begin{bmatrix} A^{cof} & A^{DCBs} & A^{DCBr} \end{bmatrix} \begin{bmatrix} X^{cof} \\ X^{DCBs} \\ X^{DCBr} \end{bmatrix}, \quad (10)$$

where A represents the transfer matrix, X^{cof} represents the ionospheric model coefficients, X^{DCBs} and X^{DCBr} represents all satellites' and receivers' DCB, respectively. For the two-step ionospheric modeling algorithm, the reference station's DCBs for each satellite X_S^{DCBr} were estimated, while the rover stations' DCBs were expressed as the linear combinations of the prior $\Delta(D_1^r - D_2^r)$ products and X_S^{DCBr} coefficients during the estimation process; the mathematical model is as follows:

$$STEC = AX = \begin{bmatrix} A^{cof} & A^{DCBs} & A_S^{DCBr} \end{bmatrix} \begin{bmatrix} X^{cof} \\ X^{DCBs} \\ X_S^{DCBr} \end{bmatrix}, \quad (11)$$

The reference station plays an extremely important role in the new algorithm, and it is strongly recommended to perform data quality analysis before ionospheric modeling to ensure model accuracy. It should be noted that, in order to simplify the analysis above, only the co-location (or distance ultra short) stations were chosen; the effects of the atmospheric delay could be entirely eliminated by the differential method in specific situations. In the actual ionosphere mod-

Fig. 4 Monthly $\Delta(D_1^{r\wedge} - D_2^r)$ values and variations of all GLONASS satellites for four groups of GLONASS co-location stations

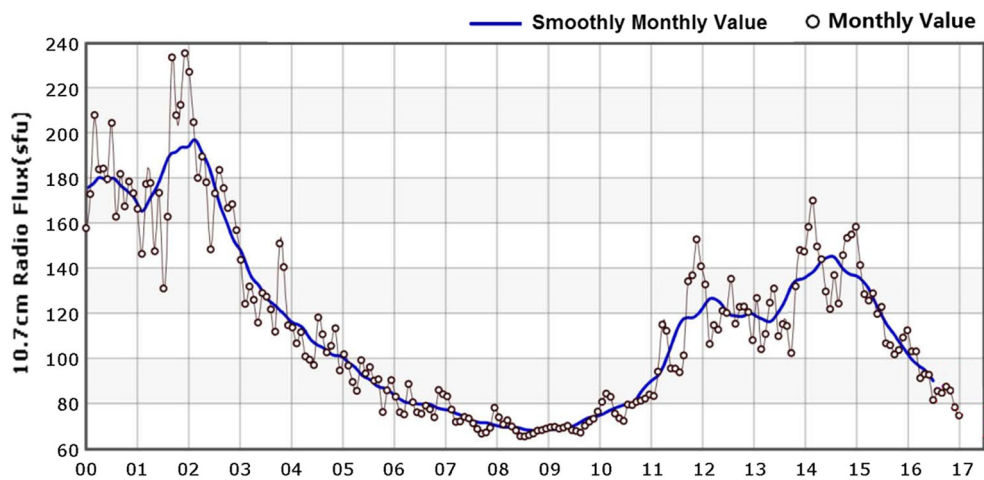
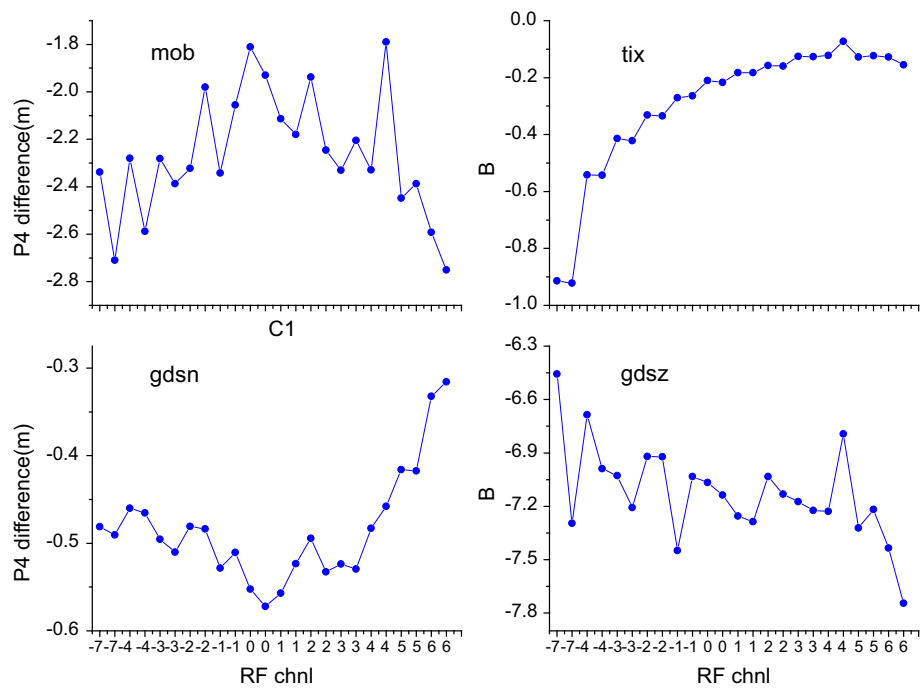


Fig. 5 Solar cycle F10.7 cm radio flux progression (<http://www.swpc.noaa.gov/phenomena>)

eling process, the distance between the reference and rover station cannot be ignored, so a prior ionosphere product had to be introduced to obtain a reliable $\Delta(D_1^{r\wedge} - D_2^r)$ product.

5 Experimental analysis

5.1 Experimental data

As is known, TEC is strongly controlled by the solar activity in a rather complicated way (Liu et al. 2006). In order to evaluate the effectiveness of our proposed ionospheric modeling approach in different space environments, we selected two typical periods. According to Fig. 5, data of DoY 234-248,

2009 were chosen because of low solar activity, while data of DoY 066-080 2014 were chosen because of the high solar activity. About 86 GPS/GLONASS stations from the EUREF Permanent Network were analyzed. Figure 6 shows the station distribution in 2009 (a few stations changed the receivers in 2014), and Table 2 gives an overview of the number and types of receivers used.

By considering the geographic and receiver type factors, the BERG station was chosen as the reference station. It was located at N 46.499°, E 11.337°, and equipped with the LECIA GRX1200GGPRO receiver. In the experiments, a considerable number of stations (all Leica and Trimble receivers) were lacking P1 observations and there was no accurate C1-P1 DCB product available for GLONASS till

Fig. 6 Selected station distributions in 2009

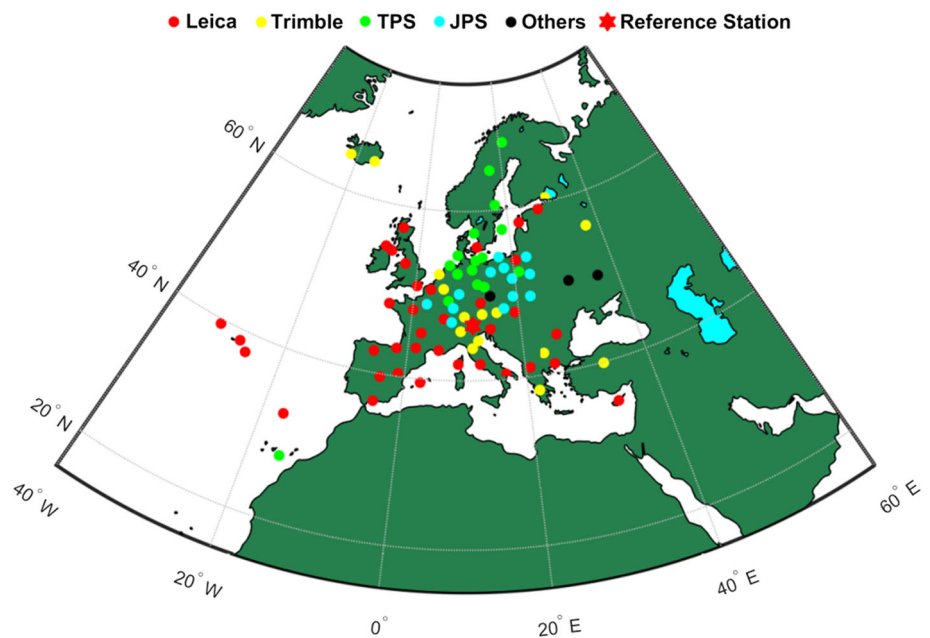


Table 2 Number and receiver types of the selected stations

2009, DOY 234-248		2014, DOY 066-080	
Manufacturers	Station numbers	Manufacturers	Station numbers
LEICA	38	LEICA	41
TRIMBLE	13	TRIMBLE	14
TPS	16	TPS	13
JPS	16	JPS	14
NOV	2	NOV	2
ASHTECH	1	JAVAD	2
Total	86		

now. So the GLONASS C1 observations were used instead, and the GLONASS C1P2 DCB parameters were estimated during the experiments.

5.2 IFB analysis

Figures 7 and 8 show the average and STD of $\Delta(D_1^{\wedge} - D_2^r)$ values for all 85 rover stations in 2009 and 2014 (each column represents a single station). Due to the distance between reference and rover station, we chose the JPL ionospheric products as the prior ionosphere information to estimate the $\Delta(D_1^{\wedge} - D_2^r)$ value for each rover station. Similar to our previous analysis, the $\Delta(D_1^{\wedge} - D_2^r)$ values varied because of the different receiver manufacturers and types. The daily $\Delta(D_1^{\wedge} - D_2^r)$ values showed excellent stability in 2009, STDs of over 76.3% stations were within 0.1 m (over 91.7% were within 0.2 m). The estimated $\Delta(D_1^{\wedge} - D_2^r)$ values will be affected by the prior ionospheric product due to the intense solar activity; the results were relatively poorer in 2014. STDs

of only 47.8% were within 0.1 m, but still over 88.7% were within 0.2 m.

5.3 Ionospheric model and satellite DCB analysis

During the experiments, we chose a spherical harmonic function of order four to express the regional ionospheric distribution. A set of ionospheric model coefficients were estimated every 2 h with a spatial resolution of $2.5^\circ \times 5^\circ$ in the geographic latitude and longitude. The standard IONEX files were outputted with the grid range latitude 35°N – 60°N , longitude 20°W – 30°E . The satellite orbit errors were corrected by precise orbit correction provided by IGS.

Three experimental strategies were used for ionospheric modeling. In strategy A, only the GPS observations were used in the modeling process. In strategy B, the GPS and GLONASS were processed by the traditional algorithm without any IFB corrections. In strategy C, the GPS and GLONASS data were processed by the new algorithm with the prior IFB product. The estimated ionospheric model and

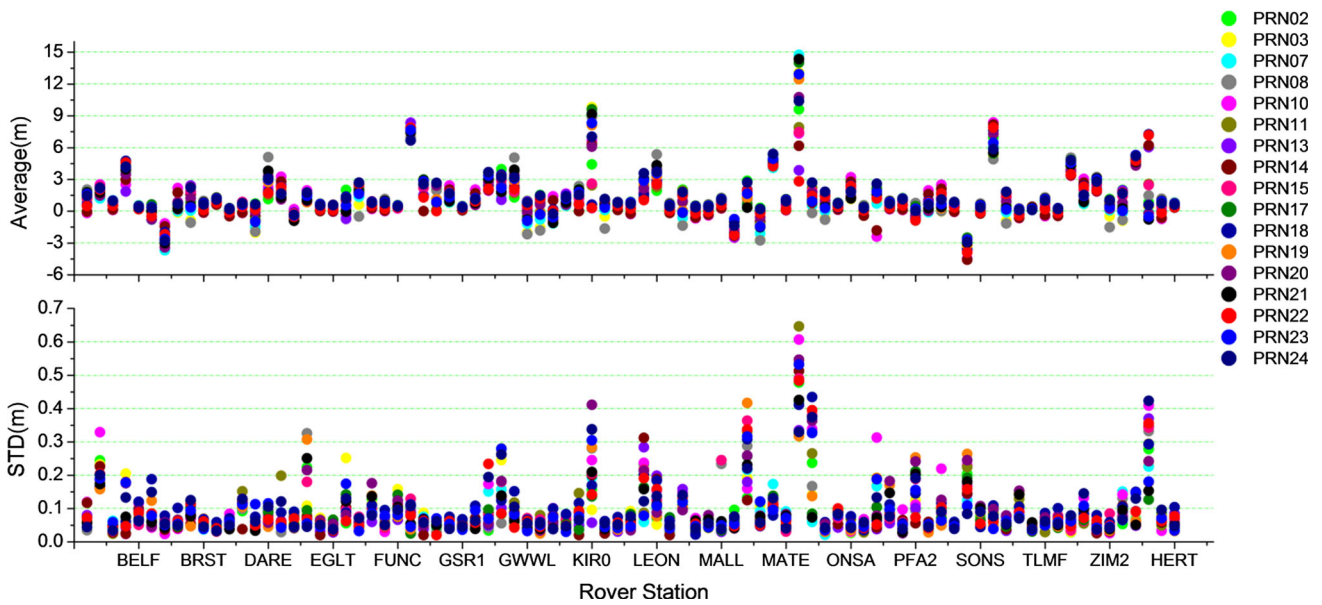


Fig. 7 Average and STD of $\Delta(D_1^r - D_2^f)$ values from DoY 234-248 in 2009 of all 85 rover stations

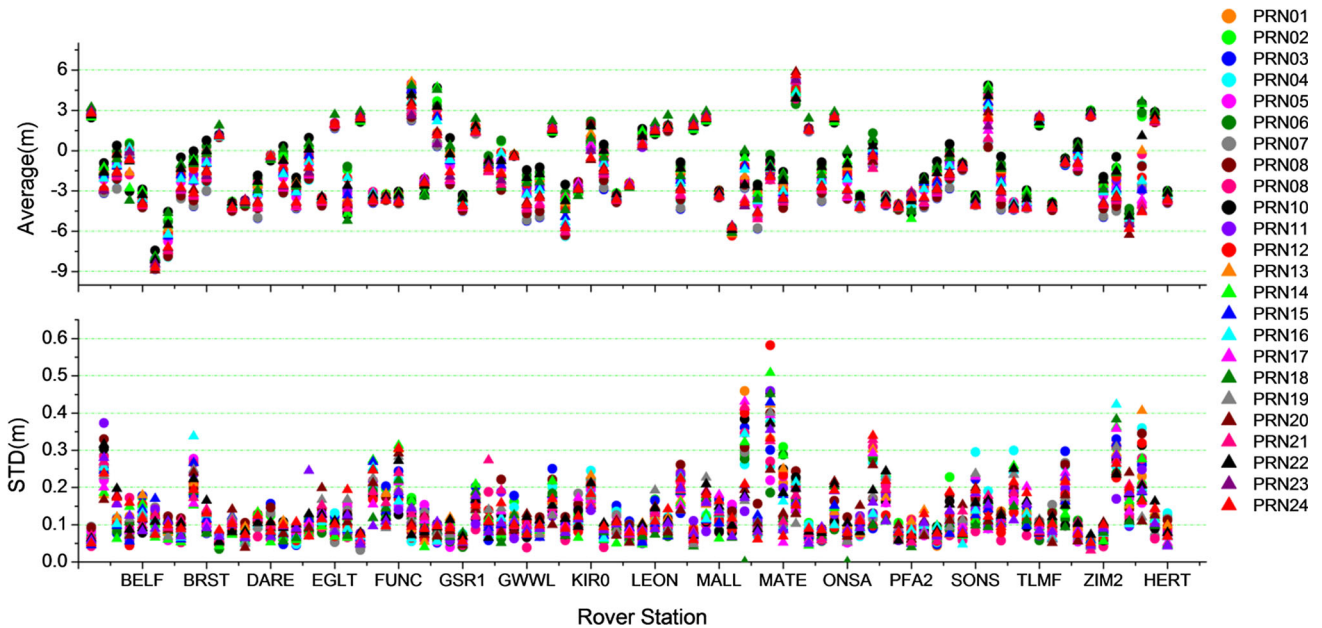


Fig. 8 Average and STD of $\Delta(D_1^r - D_2^f)$ values from DoY 066-080 in 2014 of all 85 rover stations

satellite DCB products were compared with the CODE global ionospheric products and monthly DCB products. CODE TEC is modeled in a solar-geomagnetic reference frame using a spherical harmonic expansion up to degree of order 15 (Jee et al. 2010). Figures 9 and 10 show the average and STD of model differences between strategies A, B, C and CODE for all 15 days in 2009 and 2014, respectively.

Due to the quite space environment and sufficient observations, the results of 2009 were consistent well with the CODE products. The average deviations for all 15 days were

between -1.5 TECu to 1.5 TECu, and the STDs were under 1.5 TECu. Compared with strategy A and B, the absolute average deviation of all grids decreased from 0.31 , 0.25 to 0.22 TECu with IFB correction products. However, the results of 2014 showed an obvious systematic bias in the southern region, about -2 TECu from the CODE products for all three strategies. Because the absolute ionospheric delay significantly increased, the error caused by different algorithms (including model height, mapping function and so on) increased at the same time. The average deviations for

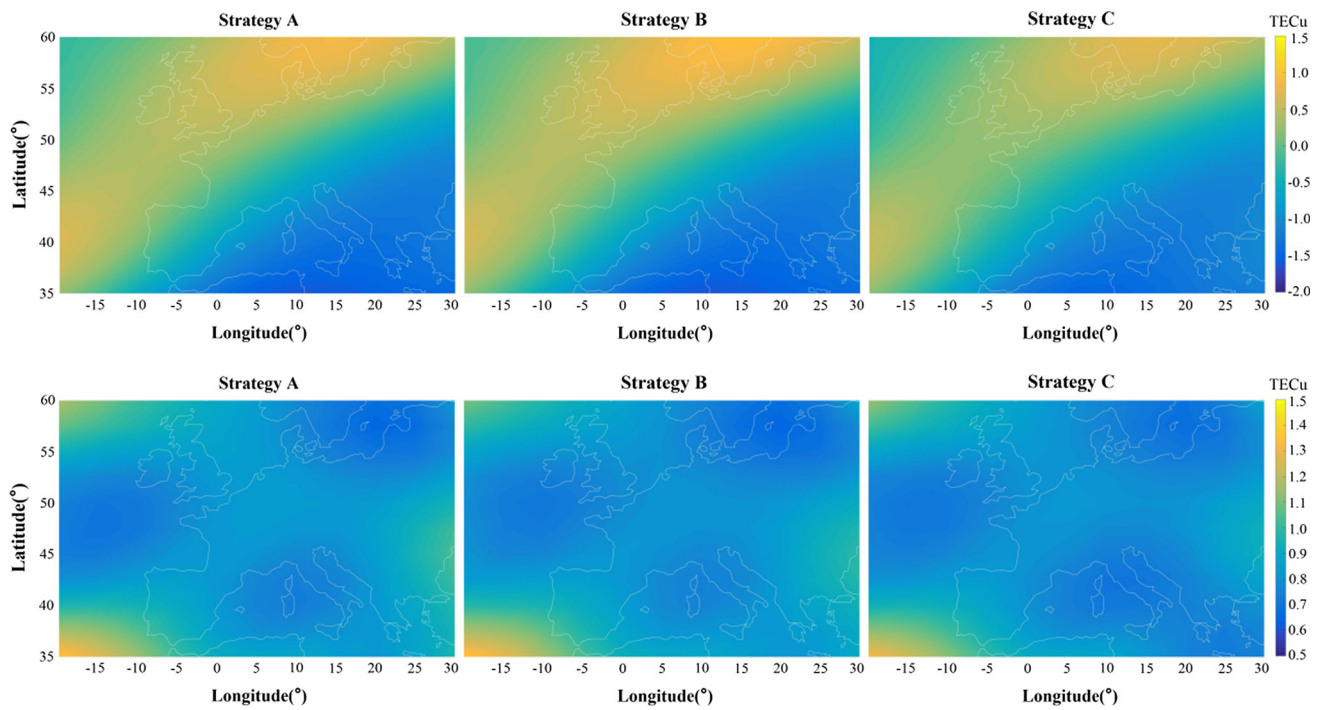


Fig. 9 Average and STD of model differences between strategies A, B, C, and CODE in 2009

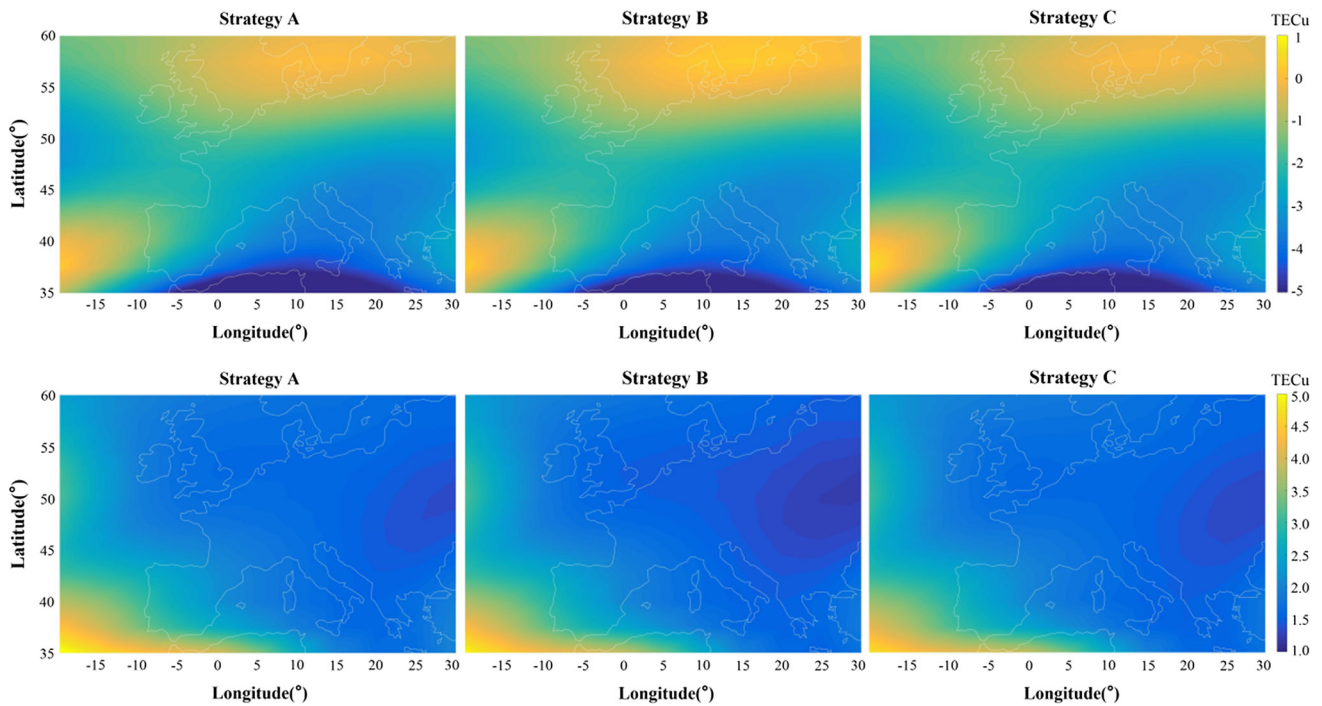


Fig. 10 Average and STD of model differences between strategies A, B, C and CODE in 2014

all 15 days were mainly between -3 TECu to 1 TECu, and the STDs were generally under 2 TECu. Similarly, the absolute average deviation of all grids for strategy C decreased from 2.20 and 2.17 TECu to 2.07 TECu compared with strategy A and B.

The satellite and receiver DCB per day were obtained as a by-product of the ionospheric modeling. The DCB accuracy and stability can reflect the ionospheric model accuracy to some extent. Figure 11 shows the RMS of the difference between the estimated GPS satellite DCB and CODE

Fig. 11 GPS satellite DCB RMS between strategies A, B, C, and CODE in 2009 and 2014

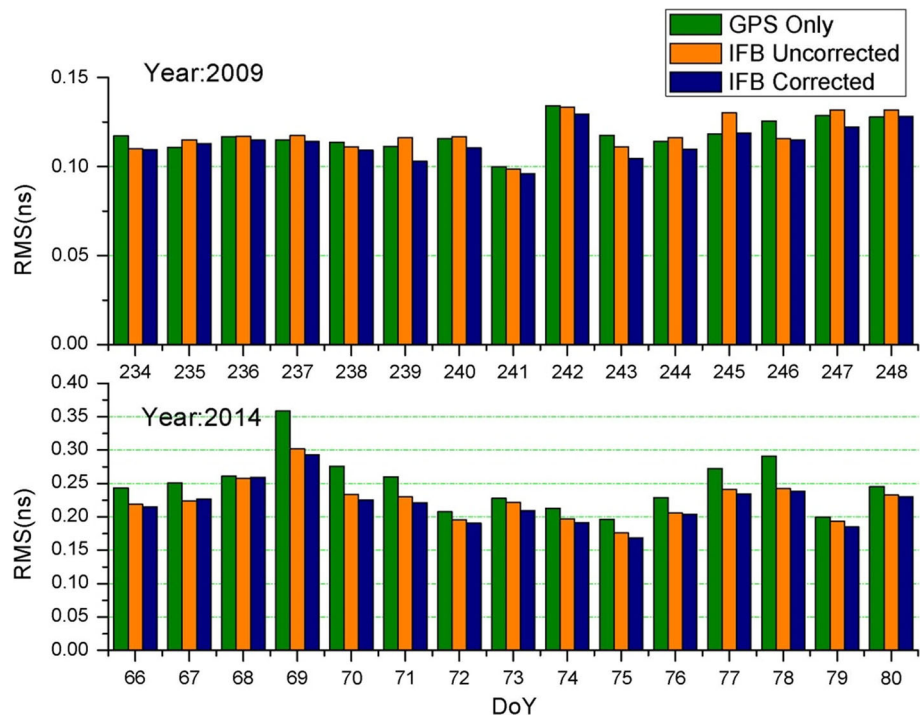
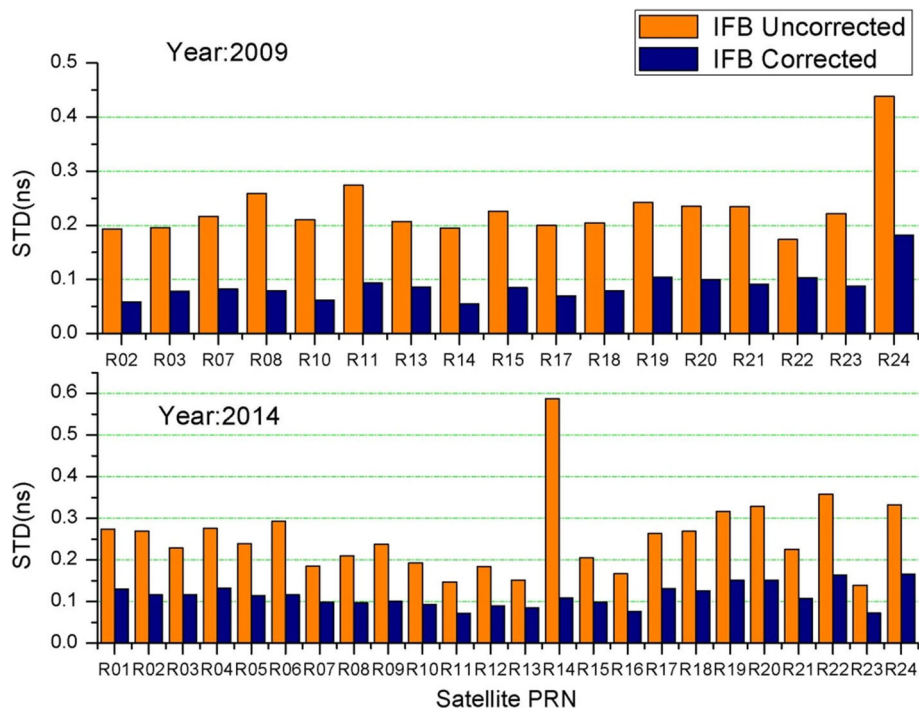


Fig. 12 GLONASS satellite DCB STD of strategies B, C in 2009 and 2014



monthly products during all 30 days. The results of 2009 were very consistent with the CODE products, the average RMS of strategy A and strategy B were 0.118 ns, with the IFB correction product, the average RMS of strategy C decreased by 4.2% to 0.113 ns. By contrast, the valuation accuracy of 2014 was seriously affected by the solar activity and showed more clear distinctions. The average RMS

of strategy A was 0.249 ns, which was the lowest precision because of the fewest observations. The average RMS of strategy B decreased by 9.6% compared to strategy A, because of the greater number of observations. With the IFB correction, the average RMS of strategy C decreased to 0.219 ns with an improvement of 2.4% compared to strategy B.

At the present, there are no other agencies which can provide GLONASS C1P2 satellite DCB products; we could only assess the inner precision for all the two selected periods. Figure 12 shows the GLONASS satellite DCB STD of strategies B, C in 2009 and 2014. The estimated accuracies of both years were significantly improved because of the IFB correction products; for 2009, the average STD decreased by 61.9% from 0.231 ns to 0.088 ns, while for 2014, the average STD decreased by 55.4% from 0.253 ns to 0.113 ns, which demonstrated the great influence of the GLONASS pseudo-range IFB on the ionospheric model and DCB estimation.

6 Conclusion

In this paper, we used the co-location GLONASS data to analyze the effects of the pseudo-range IFB on the ionospheric delay values and proposed a new two-step ionosphere modeling method to eliminate their adverse effects. The experimental results showed the GLONASS P1P2 pseudo-range IFB varied between the different satellites, and did not exhibit a linear relationship between the frequencies for all the types of receiver combinations. Through the experiments of two typical solar activity periods, the new method was demonstrated to be able to weaken the influence of the GLONASS pseudo-range IFB on the ionospheric model and DCB estimation. The absolute average deviation of TEC decreased from 0.31 to 0.22 TECu (TEC unit) for low solar activity, while from 2.20 to 2.07 TECu for high solar activity. The improvement in estimation accuracy of GPS satellite DCB was strongly related to the solar activity. For low solar activity, the average RMS decreased by about 4%, while for high solar activity the average RMS decreased from 0.249 ns to 0.219 ns, due to the increase of observations and IFB correction. Moreover, with the IFB correction, GLONASS satellite DCB estimation accuracy can reach up to about 0.1 ns with a great improvement of over 55% in both space environments. Based on the above discussion, we suggest choosing the same type of GLONASS receivers or using the two-step algorithm proposed in this paper during ionospheric modeling with GLONASS observations.

Acknowledgements This study was funded by National Natural Science Foundation of China (41604017 and 41404010), National Key Research and Development Plan (2016YFD0800301), as well as Science and Technology Planning Project of Guangdong Province (2013B020314016 and 2015B010110006).

References

- Al-Shaery A, Zhang S, Rizos C (2013) An enhanced calibration method of GLONASS inter-channel bias for GNSS RTK. *GPS Solut* 17(2):165–173
- Arikan F, Nayir H, Sezen U et al (2008) Estimation of single station interfrequency receiver bias using GPS-TEC. *Radio Sci.* doi:10.1029/2007rs003785
- Bassiri S, Hajj GA (1992) Modeling the global positioning system signal propagation through the ionosphere. *Telecommunications and Data Acquisition Progress Report 42-110: 92-103*, NASA Jet Propulsion Laboratory, Caltech, Pasadena
- Bilitza D, Reinisch BW (2008) International reference ionosphere 2007: improvements and new parameters. *Adv Space Res* 42(4):599–609
- Camargo PO, Monico JFG, Ferreira LDD (2000) Application of ionospheric corrections in the equatorial region for L1 GPS users. *Earth Planets Space* 52(11):1083–1089
- Chuang S, Wenting Y, Weiwei S et al (2013) GLONASS pseudo-range inter-channel biases and their effects on combined GPS/GLONASS precise point positioning. *GPS Solut* 17(4):439–451
- Dow JM, Neilan RE, Rizos C (2009) The international GNSS service in a changing landscape of global navigation satellite systems. *J Geod* 83(3–4):191–198
- Håkansson M, Jensen ABO, Horemuz M et al (2016) Review of code and phase biases in multi-GNSS positioning. *GPS Solut.* doi:10.1007/s10291-016-0572-7
- Heise S, Stolle C, Schlüter S et al (2005) Differential code bias of GPS receivers in low earth orbit: an assessment for CHAMP and SAC-C[M]/Earth Observation with CHAMP. Springer, Berlin, pp 465–470
- Hernández-Pajares M, Juan JM, Sanz J et al (2009) The IGS VTEC maps: a reliable source of ionospheric information since 1998. *J Geod* 83(3–4):263–275
- Hernández-Pajares M, Juan JM, Sanz J, Aragón-Ángel A, García-Rigo A, Salazar D, Escudero M (2011) The ionosphere: effects, GPS modeling and the benefits for space geodetic techniques. *J Geod* 85(12):887–907
- Hong CK, Grejner-Brzezinska DA, Kwon JH (2008) Efficient GPS receiver DCB estimation for ionosphere modeling using satellite-receiver geometry changes. *Earth Planets Space* 60(11):e25–e28
- Jakowski N, Heise S, Wehrenpfennig A et al (2002) GPS/GLONASS-based TEC measurements as a contributor for space weather forecast. *J Atmos Solar-Terr Phys* 64(5):729–735
- Jee G, Lee HB, Kim YH et al (2010) Assessment of GPS global ionosphere maps (GIM) by comparison between CODE GIM and TOPEX/Jason TEC data: Ionospheric perspective. *J Geophys Res Space Phys.* doi:10.1029/2010JA015432
- Jin S, Luo OF, Park P (2008) GPS observations of the ionospheric F2-layer behavior during the 20th November 2003 geomagnetic storm over South Korea. *J Geod* 82(12):883–892
- Kim BC, Tinin MV (2011) Potentialities of multifrequency ionospheric correction in global navigation satellite systems. *J Geod* 85(3):159–169
- Klobuchar J (1987) Ionospheric time-delay algorithm for single frequency GPS users. *IEEE Trans Aerosp Electron Syst* 23(3):325–331
- Kozlov D, Tkachenko M, Tochilin A (2000) Statistical characterization of hardware biases in GPS + GLONASS receivers. In: *Proceedings of ION GPS*, pp 817–826
- Kunitsyn VE, Nesterov IA, Padokhin AM et al (2011) Ionospheric radio tomography based on the GPS/GLONASS navigation systems. *J Commun Technol Electron* 56(11):1269–1281
- Lachapelle G, Haggglund J, Falkenberg W, Bellemare P, Casey M, Eaton M (1986) GPS land kinematic positioning experiments. In: *Proceedings of fourth international geodetic symposium on satellite positioning*, Austin, Texas, (1986 April 28–May 2), vol 2, pp 1327–1344
- Lanyi GE, Roth T (1988) A comparison of mapped and measured total ionospheric electron content using global positioning system and beacon satellite observations. *Radio Sci.* 23(4):483–492
- Liu L, Wan W, Ning B, Pirog OM, Kurkin VI (2006) Solar activity variations of the ionospheric peak electron density. *J Geophys Res* 111(8):A08304. doi:10.1029/2006JA011598

- Mannucci AJ, Wilson BD, Yuan DN, Ho CH, Lindqwister UJ, Runge TF (1998) A global mapping technique for GPS derived ionospheric total electron content measurements. *Radio Sci* 33(3):565–583
- Schaer S (1999) Mapping and Predicting the Earth's Ionosphere Using the global positioning system. Ph.D. dissertation, Bern: The University of Bern
- Schunk RW, Scherliess L, Sojka JJ et al (2004) Global assimilation of ionospheric measurements (GAIM). *Radio Sci*. doi:[10.1029/2002RS002794](https://doi.org/10.1029/2002RS002794)
- Tsujii T, Harigae M, Inagaki T et al (2000) Flight tests of GPS/GLONASS precise positioning versus dual frequency KGPS profile. *Earth Planets Space* 52(10):825–829
- Wanninger L, Wallstab-Freitag S (2007) Combined processing of GPS, GLONASS, and SBAS code phase and carrier phase measurements. In: *Proceedings of ION GNSS, MLA*, pp 866–875
- Wanninger L (2012) Carrier-phase inter-frequency biases of GLONASS receivers. *J Geod* 86(2):139–148
- Wild U (1994) Ionosphere and geodetic satellite systems: permanent GPS tracking data for modeling and monitoring. *Geod Geophys Arb Schweiz* 48:48
- Yamanda H, Takasu T, Kubo N, Yasuda A (2010) Evaluation and calibration of receiver inter-channel biases for RTK-GPS/GLONASS. In: *Proceedings of ION GNSS*, pp 1580–1587
- Zinoviev AE (2005) Using GLONASS in combined GNSS receivers: current status. In: *Proceedings of ION GNSS*, pp. 1046–1057